Resources, Conservation & Recycling 195 (2023) 106997

Contents lists available at ScienceDirect

Resources, Conservation & Recycling

journal homepage: www.elsevier.com/locate/resconrec

Seasonal and regional changes in terrestrial carbon uptake under an overshoot scenario

Wei Cheng [a,b,*], Lei Huang [c], Zhu Liu [c], Jinwei Dong [a,b,d], John C. Moore [e,f,g], Douglas G. MacMartin [h], Xiangzheng Deng [a,b,d,*]

[a] Institute of Geographic Sciences and Natural Resources Research, Chinese Academy of Sciences, Beijing, 100101, China
[b] Key Laboratory of Land Surface Pattern and Simulation, Chinese Academy of Sciences, Beijing, 100101, China
[c] Department of Earth System Science, Ministry of Education Key Laboratory for Earth System Modeling, Institute for Global Change Studies, Tsinghua University, Beijing, 100084, China
[d] University of Chinese Academy of Sciences, Beijing, 100049, China
[e] College of Global Change and Earth System Science, Beijing Normal University, Beijing, 100875, China
[f] CAS Center for Excellence in Tibetan Plateau Earth Sciences, Beijing, 100101, China
[g] Arctic Centre, University of Lapland, Rovaniemi, 96101, Finland
[h] Mechanical and Aerospace Engineering, Cornell University, Ithaca, 14850, United States of America

ARTICLE INFO

Keywords:
Climate change
Carbon dioxide removal
Terrestrial carbon uptake
Human and natural disturbance
Carbon neutrality

ABSTRACT

Carbon dioxide removal (CDR) could change terrestrial carbon uptake due to biosphere responses. Here we examine the seasonal and regional responses of net biome productivity (NBP) and its components to carbon emissions reduction under the SSP5–3.4 overshoot scenario simulated by eight CMIP6 Earth system models. Globally averaged NBP is lower under SSP5–3.4 than under SSP5–8.5, with 102±7 Pg C (51%) less accumulated during 2041 to 2100. About 59% of accumulated change in NBP is from reduction in net ecosystem productivity in the boreal growing season, associated with the reduction in atmospheric CO_2 concentrations and the resulting climate change. The rest of the accumulated reduction in NBP is due to greater disturbances from bioenergy crop expansion and land use change. These results imply that improved land management, more aggressive carbon emissions reduction and CDR will be needed to reach time flagged carbon neutrality targets after considering the adjustment in the terrestrial carbon sink.

1. Introduction

The IPCC goals of maintaining global mean temperature well below 2 °C and pursuing 1.5 °C led to the 2015 Paris set of emissions reductions pledges to reduce Greenhouse Gas (GHG) emissions. However, the pledges do not meet the IPCC targets, and typically it is assumed that carbon dioxide removal (CDR) will be required to lower GHG concentrations to achieve the temperature targets (Fuss et al., 2014; Rogelj et al., 2018). CDR refers to approaches that remove CO_2 from the atmosphere by enhancing biological or geochemical carbon sinks, or by direct air capture and long term storage (Minx et al., 2018; Keller et al., 2018). CDR could be used to compensate for GHG emissions that are difficult or costly to eliminate, and to offset earlier CO_2 emissions. Because technology is far from capable of significant negative emissions at present, achieving long-term climate goals with CDR will ramp up over many decades and so global temperatures are likely to overshoot the IPCC targets in the mid-21st century.

The climate system includes terrestrial ecosystem carbon dynamics, e.g., gross primary productivity, soil respiration and vegetation dynamics and these also act as major climate feedbacks. Idealised "pulse" removal of atmospheric CO_2 in Earth System Model (ESM) simulations show that the atmospheric CO_2 concentration rebounds due to CO_2 release from the terrestrial biosphere and the ocean due to lowered atmospheric CO_2 (Cao and Caldeira, 2010). Under low emission future scenarios, the significantly weakened carbon sinks in the ocean and land hinder the effectiveness of CDR (Jones et al., 2016; Jones and Friedlingstein, 2020). This negative feedbacks on atmospheric CO_2 levels produces further climate feedbacks through radiative forcing.

Change in terrestrial carbon uptake is partially caused by variations in terrestrial gross primary productivity (GPP) that is a cumulative rate

* Corresponding author.
E-mail addresses: chengwei@igsnrr.ac.cn (W. Cheng), dengxz@igsnrr.ac.cn (X. Deng).

https://doi.org/10.1016/j.resconrec.2023.106997
Received 15 September 2022; Received in revised form 6 April 2023; Accepted 8 April 2023
Available online 26 April 2023

over time of gross plant photosynthesis at the ecosystem level (Jung et al., 2011). Terrestrial GPP is usually jointly influenced by ecosystem plant phenology (Xia et al., 2015), photosynthetic capacity (Zhang et al., 2022), extreme climate events (Ciais et al., 2005), and disturbances (Amiro et al., 2010). The dependency of GPP variability on greenness declines with climatic humidity due to opposite dynamics between canopy structure and physiology (Green et al., 2019; Hu et al., 2022). Wang et al. (2022) explored regional and seasonal contributions to the correlations of annual land carbon uptake against terrestrial water storage and temperature using data-driven models, process-based vegetation models, and atmospheric inversions. Limitation of soil moisture can reduce GPP by ecosystem water stress and land-atmosphere interactions.

Ecosystem respiration is a major part of the terrestrial carbon cycle, which includes heterotrophic respiration (Rh) from microbial decomposition of soil organic matter and autotrophic respiration (Ra) from plants. Vegetation class determines the contributions of the autotrophic respiration and the heterotrophic respiration (Mukhortova et al., 2021). Autotrophic respiration is more sensitive to grazing and nitrogen addition than heterotrophic respiration in a meadow steppe (Shi et al., 2022). The respiration response to climate warming is mixed. Decreased autotrophic respiration under climate warming has been associated with warming-induced reduction of the winter annual productivity in a prairie caused by invasive Bromus japonicas in Southern Great Plains, USA (Li et al., 2013). The dynamics of heterotrophic respiration is related to different climatic and environmental factors, e.g., soil moisture, soil properties, temperature, soil carbon stocks, and microbial decomposition (Hawkes et al., 2017; Lei et al., 2021). Warming-related increases in soil respiration flux have been explained by increased below-ground carbon flux (Giardina et al., 2014). There is a universal decrease in the temperature sensitivity of respiration at soil temperature greater than 25 °C (Carey et al., 2016). Deadwood decomposition rates raise with temperature (Seibold et al., 2021), and the strongest temperature effect is located at high precipitation levels.

Human land use activities have produced huge changes in the biogeochemical and biophysical properties of the Earth's surface, resulting in changes in climate and other ecosystem services. In the future, land use activities are likely to expand and strengthen further to meet increasing demands for food, fiber and energy (Hurtt et al., 2020). Warmer and drier conditions particularly bring about drought, fire and insect disturbances, while warmer and wetter conditions raise disturbances from wind and pathogens (Seidl et al., 2017). Melnikova et al. (2022) explored the effects of large-scale bioenergy deployment on the climate carbon cycle feedbacks, and found increases in carbon emissions from land use change and the associated reduction in potential terrestrial carbon uptake. Although boreal forests show a generally increasing trend in resilience from CO_2 fertilization and warming, there is a significant decrease in resilience in arid, tropical and temperate forests associated with climate variability and increased water limitations (Forzieri et al., 2022; Senf et al., 2020). Forzieri et al. (2021) found about 33.4 billion tonnes of forest biomass could be seriously influenced by windthrows, fires and insect outbreaks in the period 1979–2018.

CMIP6 climate projections are simulated using the latest versions of ESMs, driven by shared socioeconomic pathway (SSP) and related to the representative concentration pathways (RCPs; Riahi et al., 2017; O'Neill et al., 2016). The SSP5–3.4 "overshoot" scenario specifies a decrease in atmospheric CO_2 concentrations after several decades of unmitigated (SSP5–8.5) emissions growth, by carbon removal which lowers radiative forcing and temperatures. Koven et al. (2022) explored the changes in the carbon cycles and climate in the overshoot scenario beyond 2100, to the year 2300. Models show a land carbon sink until the end of century but decreasing rate of carbon uptake precedes the CO_2 concentration peak due to ecosystem respiration increasing faster than increases in gross primary production, which is also related to increase in land use change emission increases caused by biofuel croplands expansion (Melnikova et al., 2022, 2021). However, there is no analysis of seasonal and regional terrestrial net biome productivity in the SSP5–3.4 overshoot scenario.

In this study, we use all eight CMIP6 ESMs which simulate the SSP5–3.4 scenario that provide the terrestrial carbon flux outputs needed to investigate the annual, seasonal, and regional features of the terrestrial biome productivity and its components in a carbon emissions reduction climate. The rest of the paper is structured as follows. In Section 2, we describe ESMs, simulation experiments, and terrestrial carbon budget. Section 3.1 includes analyses of global and regional climate changes due to carbon emissions reduction. Section 3.2 contains changes in global terrestrial productivity. Section 3.3 describes analyses of terrestrial respiration and human and natural disturbances. Section 3.4 shows terrestrial carbon uptake and atmospheric CO_2 trajectory adjustments. In Section 4, we conclude and discuss the seasonal and regional responses of terrestrial carbon uptake in the carbon emissions reduction overshoot scenario.

2. Methods

2.1. Models and simulation experiments

The eight CMIP6 ESMs which simulate the SSP5–3.4 and provide the terrestrial carbon flux outputs (Table A.1) are described in detail in Arora et al. (2020). The eight models differ in respect of the structure and the representation of carbon cycle processes. In these models, five models explicitly represent the nitrogen cycle coupling to their carbon cycle: ACCESS-ESM1–5, CESM2-WACCM, CMCC-ESM2, MIROC-ES2L and UKESM1–0-LL. UKESM1–0-LL has a land model that simulate vegetation cover dynamically with competition between plant functional types (Sellar et al., 2019). We use one ensemble member of each model for the analysis to weight the ESMs equally.

The SSP5–8.5 scenario shows radiative forcing close to specified in the RCP8.5 scenario of 8.5 W m^{-2} in 2100, which represents the no-mitigation end of the range of future pathways (O'Neill et al., 2016). SSP5 is characterized by material-intensive consumption, and rapid and resource-intensive development patterns (Kriegler et al., 2017). SSP5–3.4 scenario fills a gap in existing Earth system simulations by exploring the impacts of a substantial 21st century overshoot in radiative forcing. This SSP5–3.4 scenario follows the SSP5–8.5 unmitigated scenario, through to 2040, at which point aggressive mitigation is undertaken to rapidly decrease carbon emissions to zero by around 2070 and to net negative levels thereafter. The two SSP5 scenarios permit an evaluation of possible changes in the climate system, impacts on ecosystems, and the effectiveness of mitigation by carbon emissions reduction.

2.2. Terrestrial carbon budget

In the terrestrial ecosystem, the carbon budget can be expressed, based on the Intergovernmental Panel on Climate Change (Watson et al., 2000) as:

$$GPP = NPP + R_a = NEP + R_h + R_a = NBP + disturbance + R_h + R_a \quad (1)$$

where *GPP* represents the gross primary productivity, *NPP* is the net primary productivity, R_a is the autotrophic respiration, *NEP* is the net ecosystem productivity, R_h is the heterotrophic respiration, *NBP* represents the net biome productivity, and *disturbance* includes anthropogenic emissions from land cover and land use changes, fires and crop harvest. In this study, *NBP*, *NEP*, *GPP*, *NPP*, R_a, and R_h are direct outputs from simulations, while *disturbance* is estimated by subtracting *NBP* from *NEP*. We use *NBP* to inspect the carbon storage flux in terrestrial ecosystems. A positive *NBP* value represents atmospheric CO_2 is sequestered in the terrestrial ecosystem, while a negative *NBP* value indicates carbon releases from the terrestrial ecosystem to the atmosphere.

A fixed ratio of 1:2.13 is used to covert the carbon amount (unit: Pg C) released from or stored in the terrestrial ecosystem to the equivalent amount of airborne CO_2 mole fractions (unit: ppm; Clark, 1982; O'Hara, 1990).

2.3. Statistical analyses

In subsequent analyses, we utilize the multi-model mean of the SSP5–8.5 simulations during 2015–2025 as the baseline for comparisons with the SSP5–8.5 runs and the SSP5–3.4 runs during 2081–2100. These changes represent the responses to a carbon removal and global warming compared with current climate state, respectively. Change in SSP5–3.4 is compared with SSP5–8.5 at the end of this century, which exhibits the response under carbon emissions reduction relative to business as usual. Differences are quoted with a range denoting the standard error in the difference.

The model outputs are quite Normally distributed, and we utilize Student's *t*-test at each grid point on the maps in the figures A.16 and A.17. Stippling shows regions where changes are statistically significant at the 5% level. The Null hypotheses are "perturbated run = baseline" over the 20 years period. The returned probability for each grid is two-tailed. Stippling in other maps denotes regions where fewer than five of eight models agree on the sign of the model response, when variable outputs all are available in the eight ESMs.

Changes in terrestrial carbon fluxes under the SSP5–8.5 and SSP5–3.4 simulations are computed over different regions of the globe, where the signal for terrestrial carbon flux is robust. We calculate the regional responses using the AR6 WGI reference set of land regions (Iturbide et al., 2020).

3. Results

3.1. Global and regional climate changes due to carbon emissions reduction

Surface air temperatures averaged over land are projected to be 5.6 ± 0.1 ℃ higher in SSP5–8.5 at the end of century than that during the 2015–2025 (baseline, Fig. 1) due to increase in GHG levels (IPCC, 2021). Relative to the baseline, there is a 1.9 ± 0.1 ℃ warming in SSP5–3.4 during 2081 to 2100 (Table 1). The high latitudes warm faster under both SSP5 scenarios than the tropics (Figure A.1) because of temperature feedbacks (Pithan and Mauritsen, 2014). The monthly mean surface air temperature over land increase by about 2 ℃ and 6 ℃ under SSP5–3.4 and SSP5–8.5 respectively compared with the baseline during 2081–2100, without significant monthly fluctuations (Figure A.2). The global mean surface air temperature over land is 3.7 ± 0.1 ℃ lower in SSP5–3.4 than SSP5–8.5 during 2081–2100 owing to changes in radiative forcings associated with change in CO_2 concentrations (Table 1). Largest temperature differences are at high latitudes in winter (Figure A.3).

Compared with the baseline, precipitation averaged over land increases by about 64±6 mm yr^{-1} in SSP5–8.5 during 2081–2100 (Fig. 1), caused by elevated water vapor content in the lower troposphere and change in atmospheric circulation (Bony et al., 2013; Cheng et al., 2022a; Konapala et al., 2020). The monthly mean precipitation over land increases by 20 mm yr^{-1} in June and 90 mm yr^{-1} in December under SSP5–8.5 (Figure A.2). Relative to the baseline, there is 37±6 mm yr^{-1} increase in precipitation under SSP5–3.4 during 2081–2100 (Table 1). The precipitation over land in December is about 40 mm yr^{-1} greater under SSP5–3.4 than the baseline (Figure A.2). Increase in precipitation appears in the mid-high latitudes over land, the equatorial region and the Southern Ocean in SSP5–3.4. Relative to the baseline, annual mean precipitation increases by over 8% in the northwestern North America, Tibetan Plateau and East Asia under SSP5–3.4, and the precipitation during June-July-August (JJA) is over 200 mm yr^{-1} higher in both

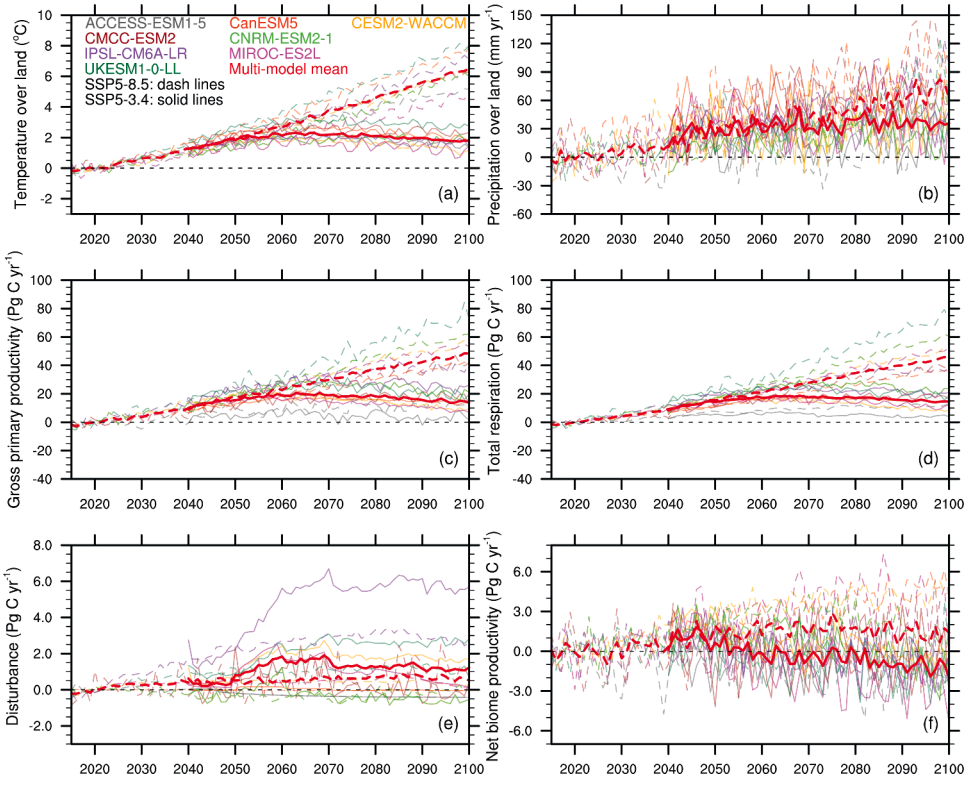

Fig. 1. Annual mean time evolution of changes in surface air temperature over land (℃, a), precipitation over land (mm yr^{-1}, b), gross primary productivity (GPP, Pg C yr^{-1}, c), Total (autotrophic and heterotrophic) respiration (TR, Pg C yr^{-1}, d), disturbance (NEP-NBP, Pg C yr^{-1}, e) and net biome productivity (NBP, Pg C yr^{-1}, f) of each ESM (colored lines) and multi-model mean (red lines) for the 21st century in SSP5–8.5 (dashed lines) and SSP5–3.4 (solid lines) scenarios. Changes are relative to the average of SSP5–8.5 during 2015–2025.

Table 1
Annual mean changes in climate and terrestrial carbon fluxes. Numbers represent changes in SSP5–8.5 and SSP5–3.4 in 2081–2100 relative to the average of SSP5–8.5 during 2015–2025 (baseline), and changes in SSP5–3.4 compared with SSP5–8.5 in 2081–2100. ±range indicates the cross-model standard error of the eight ESMs in estimating the change. Percentage values represent changes divided by the baseline value. Radiative fluxes in the downward direction are positive. Positive values for gross primary productivity (GPP), net primary productivity (NPP), net ecosystem productivity (NEP) and net biome productivity (NBP) represent carbon sequestration in ecosystems, while negative values indicate carbon releases to the atmosphere; the opposite applies to total respiration (TR), autotrophic respiration (AR), heterotrophic respiration (HR) and disturbance.

Variable	SSP5–8.5 relative to baseline		SSP5–3.4 relative to baseline		SSP5–3.4 relative to SSP5–8.5	
	Change	Percentage	Change	Percentage	Change	Percentage
Surface air temperature over land (°C)	5.6 ± 0.1	55.6 ± 0.7%	1.9 ± 0.1	18.9 ± 0.7%	-3.7 ± 0.1	-23.6 ± 0.4%
Precipitation over land (mm yr^{-1})	64±6	7.4 ± 0.7%	37±6	4.2 ± 0.7%	-27±8	-2.9 ± 0.8%
Surface net longwave over land (W m^{-2})	2.8 ± 0.2	4.1 ± 0.2%	-0.2 ± 0.2	-0.3 ± 0.2%	-3.1 ± 0.2	-4.6 ± 0.3%
Surface net shortwave over land (W m^{-2})	2.9 ± 0.2	2.0 ± 0.1%	3.4 ± 0.1	2.3 ± 0.1%	0.5 ± 0.2	0.3 ± 0.1%
Gross primary productivity (Pg C yr^{-1})	42.9 ± 0.8	34.6 ± 0.6%	15.9 ± 0.7	12.8 ± 0.6%	-27±1	-16.2 ± 0.5%
Net primary productivity (Pg C yr^{-1})	17.4 ± 0.4	30.7 ± 0.8%	7.3 ± 0.4	12.8 ± 0.8%	-10.1 ± 0.5	-13.7 ± 0.7%
Net ecosystem productivity (Pg C yr^{-1})	2.1 ± 0.5	40±9%	0.2 ± 0.4	3 ± 8%	-1.9 ± 0.5	-26±7%
Net biome productivity (Pg C yr^{-1})	1.4 ± 0.5	86±28%	-1.0 ± 0.4	-63±26%	-2.5 ± 0.6	-80±18%
Total respiration (Pg C yr^{-1})	40.5 ± 0.5	35.0 ± 0.4%	15.7 ± 0.5	13.6 ± 0.4%	-24.8 ± 0.6	-15.9 ± 0.4%
Autotrophic respiration (Pg C yr^{-1})	25.2 ± 0.4	39.1 ± 0.6%	8.6 ± 0.4	13.3 ± 0.6%	-16.6 ± 0.4	-18.5 ± 0.5%
Heterotrophic respiration (Pg C yr^{-1})	15.3 ± 0.2	29.9 ± 0.5%	7.1 ± 0.2	14.0 ± 0.4%	-8.1 ± 0.3	-12.3 ± 0.4%
Disturbance (Pg C yr^{-1})	0.7 ± 0.1	19±2%	1.2 ± 0.1	33±2%	0.5 ± 0.1	12±2%
Canopy transpiration (mm yr^{-1})	-15±1	-6.6 ± 0.5%	5 ± 1	2.0 ± 0.5%	20±1	9.2 ± 0.5%
Soil liquid water (kg m^{-2})	61±1	5.3 ± 0.1%	26±1	2.2 ± 0.1%	-36±2	-2.9 ± 0.1%

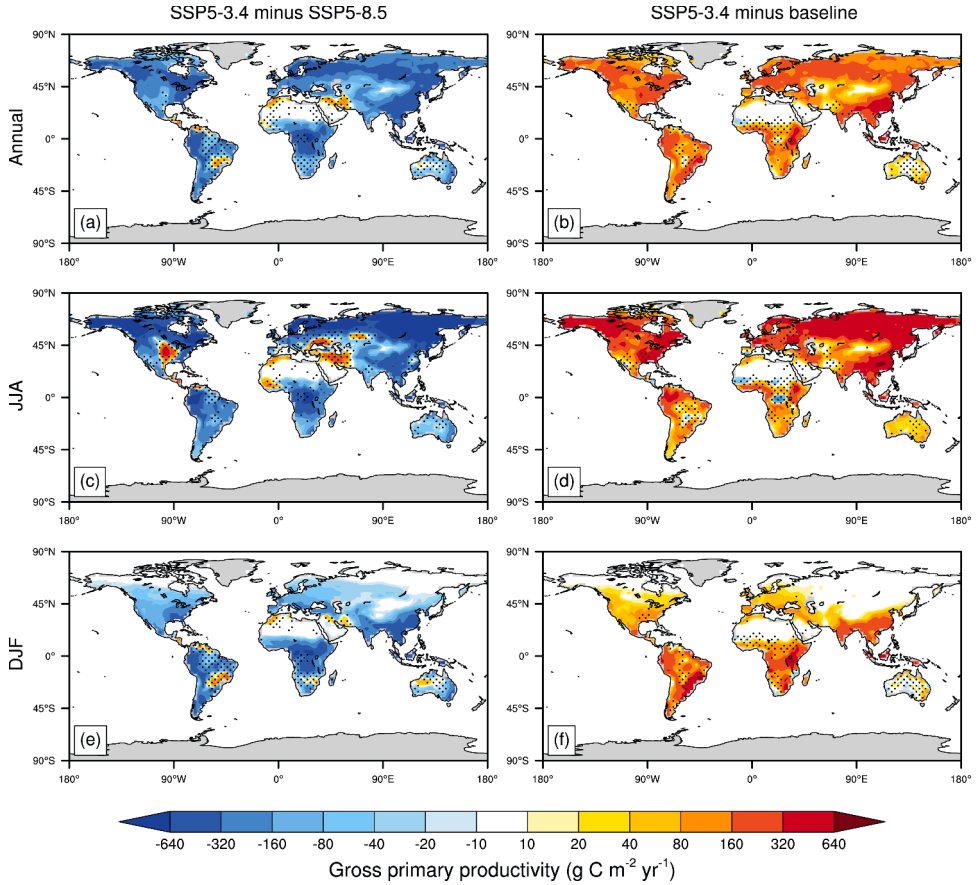

Fig. 2. Maps showing simulated (a and b) annual average, (c and d) JJA mean, and (e and f) DJF mean changes in gross primary productivity (g C m^{-2} yr^{-1}) under the SSP5–3.4 multi-model mean compared with SSP5–8.5 during 2081–2100 (Left) and under the SSP5–3.4 multi-model mean compared with the baseline (SSP5–8.5 during 2015–2025, Right). Stippling denotes regions where fewer than five of eight models agree on the sign of the model response.

Tibetan Plateau and East Asia. Carbon emissions reduction under SSP5–3.4 compensates for zonal mean change in precipitation under climate warming in SSP5–8.5, especially in the mid-high latitudes (Figures A.1 and A.4). The global mean precipitation over land is 27±8 mm yr^{-1} lower in SSP5–3.4 than SSP5–8.5 during 2081–2100 (Table 1), which is consistent with cooling effect due to change in CO_2 concentrations. In December-January-February (DJF), precipitation over land decreases by 47±11 mm yr^{-1} under SSP5–3.4, however the change is not statistically significant in JJA (Tables A.2 and A.3). Relative to SSP5–8.5, there are 23%, 19% and 17% increases in annual precipitation under SSP5–3.4 in southern Central America, Northern South America and Mediterranean, respectively, with stronger increase in precipitation during JJA (Figure A.4).

3.2. Global terrestrial productivity

Global mean gross primary productivity (GPP) for both SSP5–8.5 and SSP5–3.4 substantially are 42.9 ± 0.8 Pg C yr^{-1} and 15.9 ± 0.7 Pg C yr^{-1} separately greater than the baseline, consistent with rising atmospheric CO_2 levels (Figs. 1 and A.5, Table 1). Relative to the baseline, the monthly mean GPP under SSP5–8.5 increases by about 65 Pg C yr^{-1} in June and 30 Pg C yr^{-1} in December (Figure A.2). There is about 25 Pg C yr^{-1} increase in GPP over land in June and 10 Pg C yr^{-1} in December under SSP5–3.4. GPP increases by 40–600 g C m^{-2} yr^{-1} in the vegetation covered area during the growing season under SSP5–3.4, which is related to warming effect from higher CO_2 concentrations than the baseline and increases in surface net shortwave flux (Figures A.3, A.5 and A.6). The global mean GPP is 27±1 Pg C yr^{-1} lower in SSP5–3.4 than SSP5–8.5, associated with reduction in atmospheric CO_2 levels and cooling effect (Table 1). In JJA, GPP decreases by 34±1 Pg C yr^{-1} under SSP5–3.4, and there is an 18±1 Pg C yr^{-1} reduction in DJF (Tables A.2 and A.3). Carbon emissions reduction under SSP5–3.4 weakens GPP, especially at the tropics and mid-latitudes (Tables 1 and 2, Figure A.1). There are decreases in GPP under SSP5–3.4 compared with SSP5–8.5 on the most of vegetated land area (Fig. 2), except Central North America in JJA related to increase in precipitation.

Net primary productivity (NPP) is computed by the exclusion of autotrophic respiration (see Section 3.3) from GPP. Relative to the baseline, NPP for both SSP5–8.5 and SSP5–3.4 substantially increase by 17.4 ± 0.4 Pg C yr^{-1} and 7.3 ± 0.4 Pg C yr^{-1} respectively, because of a larger increase in gross primary productivity than the increase in autotrophic respiration (Table 1, Figure A.7). The monthly mean NPP under SSP5–8.5 increases by about 32 Pg C yr^{-1} in May and less than 10 Pg C yr^{-1} in December (Figure A.2). Compared with baseline, there is about 12 Pg C yr^{-1} increase in NPP over land in June and 5 Pg C yr^{-1} in December under SSP5–3.4. Compared with SSP5–8.5, the global mean NPP decreases by 10.1 ± 0.5 Pg C yr^{-1} in SSP5–3.4 during 2081–2100 (Table 1), which is dominated by the decrease in gross primary productivity from change in CO_2 concentrations. In JJA, NPP decreases by 12.1 ± 0.7 Pg C yr^{-1} under SSP5–3.4, and the reduction in DJF is 6.5 ± 0.7 Pg C yr^{-1} (Tables A.2 and A.3). There are decreases in NPP under SSP5–3.4 compared with SSP5–8.5 in almost land area, except Central North America in JJA and at high latitudes in DJF which is mainly influenced by regional increase in GPP associated with bioenergy deployment (Melnikova et al., 2022) and reduction in autotrophic respiration, respectively (Figures A.8, A.9 and A.10).

Net ecosystem productivity (NEP) is calculated by the exclusion of heterotrophic respiration (see Section 3.3) from NPP. Relative to baseline, NEP for SSP5–8.5 increase by 2.1 ± 0.5 Pg C yr^{-1}, associated with a smaller increase in heterotrophic respiration than the increase in net primary productivity in climate warming (Table 1, Figure A.7). The monthly mean NEP is about 15 Pg C yr^{-1} greater in May and 5 Pg C yr^{-1} lower in November under SSP5–8.5 than the baseline (Figure A.11). Relative to the baseline, change in NEP under SSP5–3.4 during 2081–2100 is not statistically significant, because the 7.3 ± 0.4 Pg C yr^{-1} increase in NPP is almost counteracted by increase in heterotrophic respiration (Table 1). However, there is about 4 Pg C yr^{-1} increase in NEP in June and 0.5 Pg C yr^{-1} reduction in December under SSP5–3.4 (Figure A.11). Compared with SSP5–8.5, the global mean NEP decreases by 1.9 ± 0.5 Pg C yr^{-1} in SSP5–3.4 during 2081–2100 (Table 1), associated with a larger decrease in NPP than the decrease in autotrophic respiration in carbon emissions reduction. In JJA, NEP decreases by 2.7 ± 0.7 Pg C yr^{-1} under SSP5–3.4, and the change in DJF is not statistically significant (Tables A.2 and A.3, Figure A.9). There are increases in NEP under SSP5–3.4 compared with SSP5–8.5 at mid-high latitudes of northern hemisphere in DJF (Figures A.9 and A.12) consistent with decrease in respiration under the SSP5–3.4 overshoot scenario.

3.3. Terrestrial respiration and human and natural disturbances

Global mean total respiration (TR, including autotrophic respiration and heterotrophic respiration) for both SSP5–8.5 and SSP5–3.4 substantially increase by 40.5 ± 0.5 Pg C yr^{-1} and 15.7 ± 0.5 Pg C yr^{-1} respectively relative to the baseline, owing to increases in plants primary productivity and soil organic matter (Fig. 1, Table 1). Proportion of heterotrophic respiration (HR) in TR is 38% under SSP5–8.5, and the proportion increases to 45% in SSP5–3.4 compared with the baseline, associated with vegetation dynamics (Figure A.13; Mukhortova et al., 2021). The monthly mean TR is about 55 Pg C yr^{-1} in June and 30 Pg C yr^{-1} in December greater under SSP5–8.5 than the baseline (Figure A.2). These changes are partially suppressed under SSP5–3.4, with about 20 Pg C yr^{-1} increase in TR in June and 10 Pg C yr^{-1} in December. Compared with SSP5–8.5, the global mean TR decreases by 24.8 ± 0.6 Pg C yr^{-1} in SSP5–3.4 during 2081–2100 (Table 1), and two-thirds of the change comes from the reduction in autotrophic respiration, which allows a larger decrease in TR during boreal growing season (May-August) than the other seasons (Figure A.2). In JJA, TR decreases by 31±1 Pg C yr^{-1} under SSP5–3.4, and the reduction in DJF is 18.4 ± 0.7 Pg C yr^{-1} (Tables A.2 and A.3). There are decreases in TR under SSP5–3.4 compared with SSP5–8.5 on most of land area, especially on the abundant vegetation regions e.g., eastern North America, the Amazon, Central Africa and East Asia, which is dominated by reduction in autotrophic respiration (Figs. 3, A.14 and A.15; Table 2).

Disturbance is calculated by the exclusion of NBP (see Section 3.4) from NEP, which illustrate the caron flux to air from human and natural disturbances. Relative to the baseline, global mean disturbance for both SSP5–8.5 and SSP5–3.4 increase by 0.7 ± 0.1 Pg C yr^{-1} and 1.2 ± 0.1 Pg C yr^{-1} respectively (Figs. 1, A.13 and A.16; Table 1). Relative to the baseline, the monthly mean disturbance under SSP5–8.5 increases by about 1.2 Pg C yr^{-1} in August and 0.5 Pg C yr^{-1} in December (Figure A.2). There is about 1.6 Pg C yr^{-1} increase in disturbance in June and 1 Pg C yr^{-1} in December under SSP5–3.4. Compared with SSP5–8.5, the global mean disturbance increases by 0.5 ± 0.1 Pg C yr^{-1} in SSP5–3.4 during 2081–2100 (Table 1), which is associated bioenergy crop expansion in eastern North America, western Europe and Centra Africa, and fires in Southeast Asia (Figure A.17). Change in disturbance during JJA is not statistically significant, but in DJF disturbance is 0.6 ± 0.1 Pg C yr^{-1} greater under SSP5–3.4 than SSP5–8.5 (Fig. 4, Tables A.2 and A.3). Increases in C_4 cropland area fraction under SSP5–3.4 appear in the eastern United States, Southeastern South America, Europe, western Central Asia, East Asia, and South Asia, which is associated with bioenergy crop expansion (Table 2, Figures A.16 and A.18).

3.4. NBP and atmospheric CO2 trajectory adjustments

The variations of NEP and disturbance affect the perturbations of NBP, which indicates the long-term and large-scale carbon exchanges between atmosphere and land by terrestrial ecosystems (see Eq. (1)). Relative to the baseline, NBP for SSP5–8.5 increases by 1.4 ± 0.5 Pg C yr^{-1}, because of rising atmospheric CO_2 fertilization effect (Chen et al., 2022; Table 1; Figure A.5). The global average NBP decreases by 1.0 ± 0.4 Pg C yr^{-1} in SSP5–3.4 during 2081–2100 (Table 1), which is

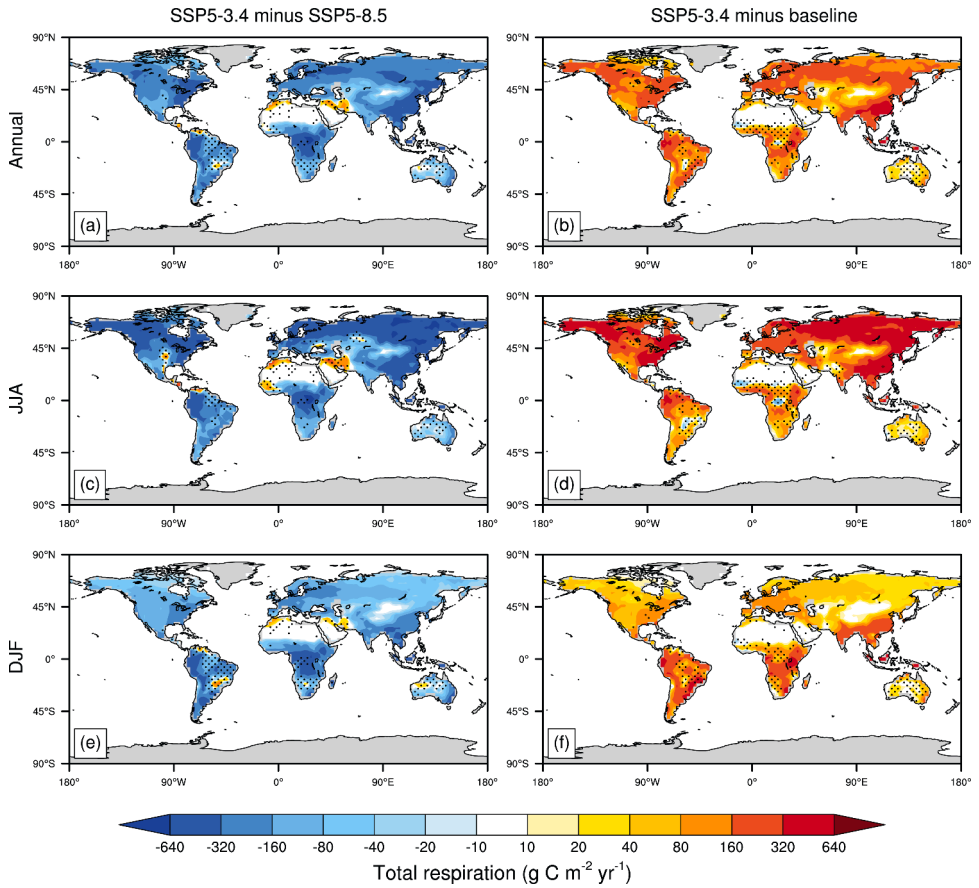

Fig. 3. Maps showing simulated (a and b) annual average, (c and d) JJA mean, and (e and f) DJF mean changes in total respiration (g C m^{-2} yr^{-1}) under the SSP5–3.4 multi-model mean compared with SSP5–8.5 during 2081–2100 (Left) and under the SSP5–3.4 multi-model mean compared with the baseline (SSP5–8.5 during 2015–2025, Right). Stippling denotes regions where fewer than five of eight models agree on the sign of the model response.

associated with 1.2 ± 0.1 Pg C yr^{-1} increase in disturbance (Fig. 4, Table 1). Relative to the baseline, the monthly mean NBP under SSP5–8.5 increases by about 12 Pg C yr^{-1} in May and decreases by 5 Pg C yr^{-1} in November (Figure A.2). There is about 2 Pg C yr^{-1} increase in NBP in May and 3 Pg C yr^{-1} reduction in November under SSP5–3.4, which indicates that carbon emissions reduction suppresses seasonal variations in the NBP under climate warming (Figure A.2).

Relative to baseline, annual mean NBP decreases by about 8–37 g C m^{-2} yr^{-1} under SSP5–3.4 in the eastern United States, northeastern South America, northern Europe, western central Africa and East Asia, which is consistent with a larger increase in total respiration and disturbance than the increase in GPP (Figs. 2, 3, 5 and A.18; Table 2). In DJF, there are decreases in NBP under SSP5–3.4 in northern North America, western South America, northern Europe, Siberia, and southern Australia, which is dominated by enhancement of total respiration under carbon emissions reduction (Figs. 3 and 5). But NBP during JJA increases by more 39 and 60 g C m^{-2} yr^{-1} in the northwestern North America and Russian Arctic region, respectively, consistent with about 2° warming and increase in gross primary productivity (Figs. 2 and A.3; Table 2).

Compared with SSP5–8.5, carbon emissions reduction in SSP5–3.4 weakens NBP in JJA with 2.7 ± 0.8 Pg C yr^{-1} reduction, and the change in DJF is not statistically significant (Tables 1, A.2 and A.3; Fig. 5). Annual mean NBP decreases by over 11–49 g C m^{-2} yr^{-1} in northern North America, the eastern United States, the western United States, southern South America, northern Europe, Siberia, and East Asia under SSP5–3.4 (Fig. 5, Table 2). NBP during JJA is over 60 g C m^{-2} yr^{-1} greater under SSP5–3.4 than SSP5–8.5 in the eastern and central United States, western Central Europe and East Asia (Fig. 5). There are increases in NBP under SSP5–3.4 in northern North America, northern Europe, and Siberia in DJF, which is dominated by reduction in total respiration under the SSP5–3.4 overshoot scenario (Figs. 5 and A.9).

The perturbations of NBP represents atmospheric CO_2 is stored in the terrestrial ecosystem or carbon releases from the terrestrial ecosystem to the atmosphere. CO_2 concentrations in SSP5–3.4 provided by integrated assessment model do not includes the terrestrial carbon feedback under carbon emissions reduction. Here, a fixed ratio of 1:2.13 is used to covert the carbon amount (unit: Pg C) released from or stored in the terrestrial ecosystem to the equivalent amount of airborne CO_2 mole fractions (unit: ppm; Clark, 1982; O'Hara, 1990). Given the assumption that the terrestrial carbon fluxes in SSP5–8.5 are in line with the specified atmospheric CO_2 trajectory, we estimate carbon absorption changes on land due to changes in radiative forcings associated with carbon emissions reduction through comparing between SSP5–3.4 and SSP5–8.5. The terrestrial carbon sequestration strength is estimated by the accumulated NBP over 2040–2100.

Fig. 6 shows the accumulated global carbon amount changes for carbon fluxes NBP, GPP, TR, NEP in Eq. (1). Relative to SSP5–8.5, decrease in accumulated NBP reaches to about 115 Pg C under SSP5.34 at the end of century. About 30% of the reduction in accumulated NBP is from the disturbance, the rest part of reduction in accumulated NBP is caused by 80 Pg C decrease in accumulated NEP. The decrease in NEP is due to a larger decrease in gross primary production than the decrease in ecosystem respiration (Fig. 6). Considering the adjustment in terrestrial carbon exchange, the decreases in accumulated NBP is equivalent to an increase of 26 ppm in 2065 and 50 ppm in 2100 relative to original concentrations in SSP5–3.4, which implies a reduced effectiveness of carbon emissions reduction from atmosphere in SSP5–3.4.

Table 2
Annual mean regional changes in terrestrial carbon fluxes. Numbers represent changes in SSP5–3.4 compared with SSP5–8.5 in a period of 2081–2100. ±range that indicates the cross-model standard error of the eight ESMs in estimating the change. Positive values for gross primary productivity (GPP) and net biome productivity (NBP) indicate carbon gains in ecosystems while negative values represent carbon losses to the atmosphere; the opposite applies to autotrophic respiration (AR), heterotrophic respiration (HR) and disturbance. Land regions used the AR6 WGI Reference Set of Land and Ocean Regions (Iturbide et al., 2020). The land regions where change in NBP is statistically significant under SSP5–3.4 compared with SSP5–8.5 are shown in this table.

Change in SSP5–3.4 relative to SSP5–8.5	Gross primary productivity (g C m^{-2} yr^{-1})	Autotrophic respiration (g C m^{-2} yr^{-1})	Heterotrophic respiration (g C m^{-2} yr^{-1})	Disturbance (g C m^{-2} yr^{-1})	Net biome productivity (g C m^{-2} yr^{-1})
Greenland/Iceland	-25±1	-14.7 ± 0.7	-8.7 ± 0.4	0.0 ± 0.1	-1.4 ± 0.5
N.W.North America	-259±11	-144±6	-86±4	-4 ± 2	-22±5
N.E.North America	-173±7	-101±4	-54±3	-3 ± 2	-11±4
W.North America	-253±26	-149±13	-78±7	-5 ± 3	-17±11
E.North America	-423±20	-259±11	-127±9	18±5	-49±14
N.W.South America	-417±18	-259±10	-111±8	6 ± 2	-43±14
N.E.South America	-169±50	-117±23	-43±14	14±3	-22±20
S.W.South America	-156±16	-89±8	-38±5	-2.4 ± 0.8	-24±6
S.South America	-171±18	-100±10	-48±4	-0.9 ± 0.6	-20±6
N.Europe	-310±14	-177±8	-95±6	-8 ± 3	-26±8
West.Central Europe	-274±27	-155±13	-88±12	-2 ± 6	-20±15
E.Europe	-283±23	-155±12	-87±9	-9 ± 13	-24±18
Mediterranean	-97±16	-58±7	-29±5	2 ± 1	-10±8
Central Africa	-401±31	-231±19	-125±11	16±4	-57±15
N.Eastern Africa	-254±28	-147±15	-90±7	2 ± 2	-17±14
S.Eastern Africa	-323±40	-179±22	-114±11	4 ± 3	-26±14
Madagascar	-276±53	-166±25	-82±17	19±2	-42±21
Russian Arctic	-207±9	-114±5	-78±3	-1.3 ± 0.2	-12±4
W.Siberia	-227±17	-122±8	-70±7	-9 ± 8	-21±12
E.Siberia	-328±14	-164±7	-113±5	-7 ± 3	-40±8
Russian Far East	-316±12	-173±6	-105±4	-1.7 ± 0.8	-33±6
E.C.Asia	-91±9	-46±5	-35±3	-1.1 ± 0.3	-8 ± 4
Tibetan Plateau	-254±9	-131±4	-93±5	-2 ± 1	-26±5
E.Asia	-428±20	-245±12	-139±10	2 ± 4	-40±15
S.E.Asia	-455±45	-269±29	-105±15	23±6	-98±22
N.Australia	-194±61	-116±36	-54±10	5 ± 2	-29±21
New zealand	-371±18	-229±11	-132±13	23±1	-29±12

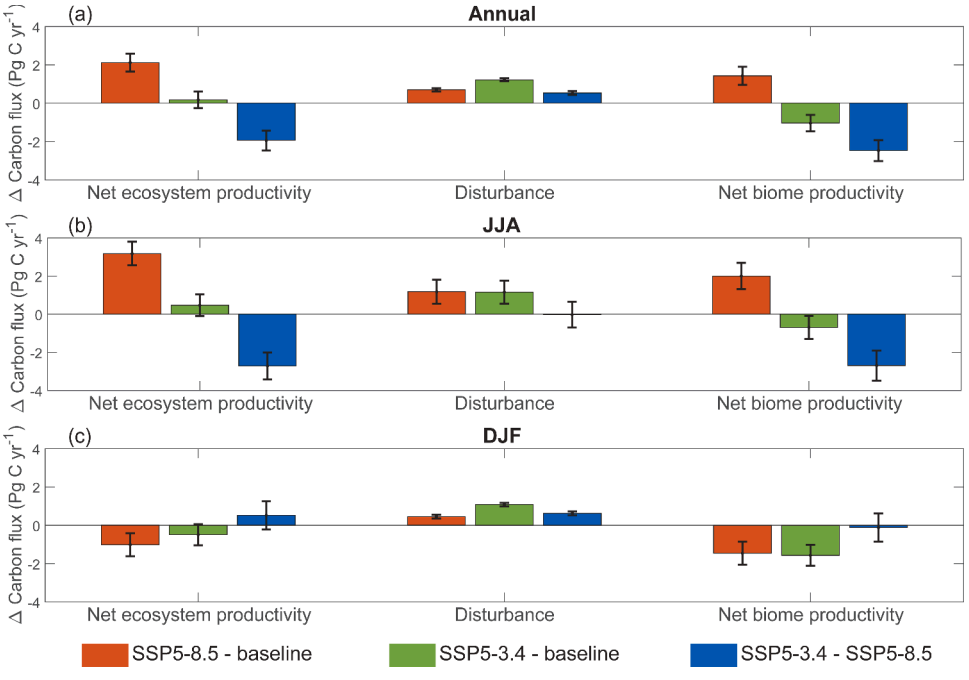

Fig. 4. Bar chart showing annual average (a), JJA mean (b), and DJF mean (c) changes in net ecosystem productivity (Pg C yr^{-1}), disturbance (Pg C yr^{-1}) and net biome productivity (Pg C yr^{-1}) under SSP5–8.5 (orange bars) and SSP5–3.4 (green bars) in 2081–2100 relative to the average of SSP5–8.5 during 2015–2025 (baseline), respectively, and changes in SSP5–3.4 compared with SSP5–8.5 in 2081–2100 (blue bars). Error bars represent standard error. Positive values for net ecosystem productivity (NEP) and net biome productivity (NBP) denote carbon sequestration in ecosystems while negative values represent carbon releases to the atmosphere; the opposite applies to disturbance.

4. Conclusions and discussion

The SSP5-3.4 overshoot scenario demands additional consideration because of its aggressive decrease in atmospheric CO_2 concentrations by net negative CO_2 emissions. We used eight CMIP6 Earth system models' simulations to investigate annual, seasonal, and regional responses of terrestrial carbon uptake and its components to the carbon emissions reduction under SSP5-3.4. Globally averaged net biome productivity is weaker under the SSP5-3.4 overshoot scenario compared with business as usual, with 102±7 Pg C reduction in accumulated net biome productivity during 2040 to 2100. The decrease in NBP, which is equivalent to 50 ppm increase in CO_2 concentration at the end of the century,

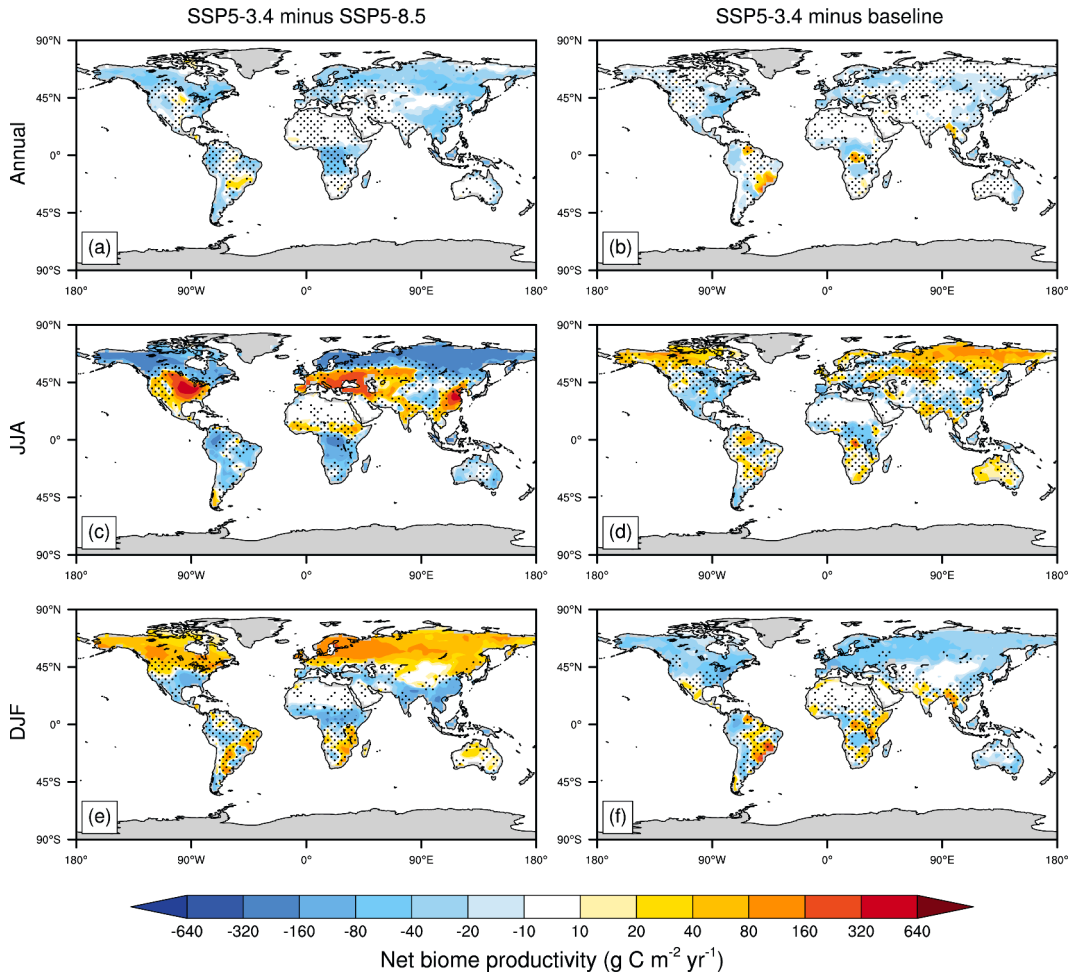

Fig. 5. Maps showing simulated (a and b) annual average, (c and d) JJA mean, and (e and f) DJF mean changes in net biome productivity (g C m^{-2} yr^{-1}) under the SSP5–3.4 multi-model mean compared with SSP5–8.5 during 2081–2100 (Left) and under the SSP5–3.4 multi-model mean compared with the baseline (SSP5–8.5 during 2015–2025, Right). Positive values denote carbon sequestration in ecosystems while negative values represent carbon releases to the atmosphere. Stippling indicates regions where fewer than five of eight models agree on the sign of the model response.

indicates a reduced effectiveness of carbon emissions reduction from atmosphere. About 59% of accumulated reduction in net biome productivity is from reduction in net ecosystem productivity during the boreal growing season (Fig. 6). The rest of the accumulated reduction in NBP could be caused by enhanced human and natural disturbances caused by bioenergy crop expansion, land use change and fires.

Net ecosystem productivity is affected by variations in terrestrial gross primary productivity and total respiration. The global mean net ecosystem productivity decreases by 1.9 ± 0.5 Pg C yr^{-1} in SSP5–3.4 relative to SSP5–8.5 during 2081–2100, associated with a larger decrease in gross primary productivity than the decrease in total respiration. However, there is about 10 g C m^{-2} yr^{-1} increases in net ecosystem productivity in northern Eurasia and northern North America during winter, which is dominated by decrease in respiration under the SSP5–3.4 overshoot scenario. Compared with SSP5–8.5, the global mean gross primary productivity decreases by 27±1 Pg C yr^{-1} under SSP5–3.4 associated with reduction in atmospheric CO_2 levels and consequent cooling effect. Terrestrial gross primary productivity is jointly controlled by ecosystem plant phenology, terrestrial water availability and photosynthetic capacity (Wang et al., 2022; Xia et al., 2015; Zhang et al., 2022). The decreases in gross primary productivity are distributed across most of the vegetated land area, except Central North America during JJA, which is related to increases in precipitation.

Change in gross primary productivity under SSP5–3.4 is related to reduction in atmospheric CO_2 levels. Change in surface CO_2 concentrations modifies cumulative rate over time of photosynthesis by altering the CO_2 gradient between intercellular and leaf surface (Chen et al., 2022), which changes photosynthesis in plants. The global annual mean 3.7 ± 0.1°C cooling from change in CO_2 concentrations also affects photosynthetic capacity. All grid cells are cooler in SSP5–3.4 compared with SSP5–8.5, but stronger cooling occurs mainly at high latitudes in winter with over 7°C cooling in northern North America and Russia Arctic regions. The reduction in surface air temperature over land is caused by changes in radiative forcings consistent with change in CO_2 concentrations and climate feedbacks (Cheng et al., 2022b). Surface net longwave over land decreases by 3.1 ± 0.2 W m^{-2} in SSP5–3.4 compared with SSP5–8.5 during 2081–2100, indicating a reduced greenhouse effect due to carbon emissions reduction. In DJF, surface net shortwave over land increases by about 0.9 ± 0.3 W m^{-2} under SSP5–3.4 compared with SSP5–8.5 associated with reduction in atmosphere moisture due to global cooling.

Water limitation also changes the growth of new cells, especially in the xylem and phloem (Gentine et al., 2019). The global mean precipitation over land decreases by 27±8 mm yr^{-1} in SSP5–3.4 relative to SSP5–8.5, which is consistent with the reduction in temperature. Limitation of soil moisture can reduce GPP by ecosystem water stress and land-atmosphere interactions (Green et al., 2019). Global mean soil liquid water is projected lower in SSP5–3.4 than that in SSP5–8.5 (Figure A.19). Relative to the SSP5–8.5, annual mean canopy transpiration increases by 20±1 mm yr^{-1} under SSP5–3.4, which is associated

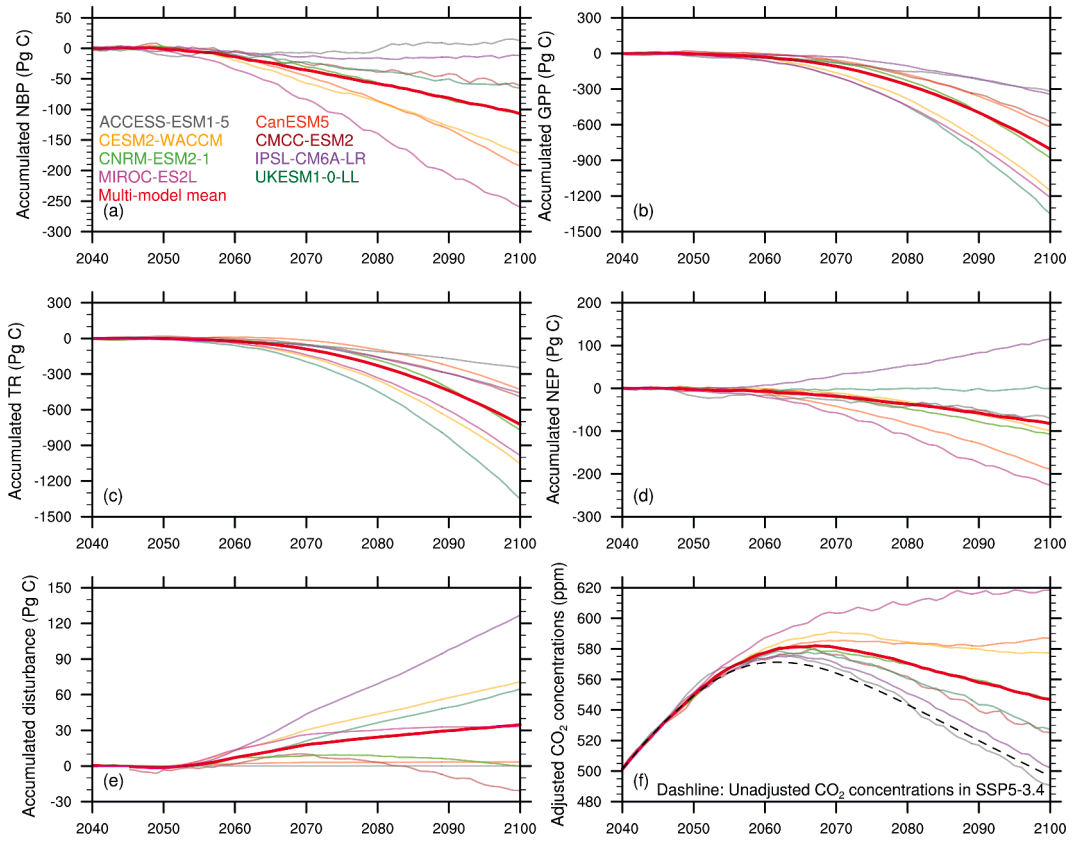

Fig. 6. The trajectories of accumulated global mean changes (Pg C) in NBP (a), GPP (b), TR (c), NEP (d), and disturbance (e) under SSP5–3.4 compared with SSP5–8.5 during 2040–2100 due to carbon emissions reduction; (f) the atmospheric CO_2 mole fraction (ppm) during 2040–2100 for SSP5–3.4 (dashed line) and the adjusted atmospheric CO_2 mole fraction due to terrestrial biogeochemistry feedbacks under SSP5–3.4 compared with SSP5–8.5. Colored line is for each ESM, and red line is for multi-model mean.

with CO_2 concentration reduction and mitigation of stomatal conductance reduction (Figure A.20). Soil moisture content provides the amount of water can be extracted by plant roots and regulates stomatal conductance (Stocker et al., 2018), which in turn affects plant water status, as well as the rate of GPP and transpiration.

Total respiration includes autotrophic respiration from plants and heterotrophic respiration. In JJA, total respiration decreases by 31±1 Pg C yr^{-1} under SSP5–3.4 compared with SSP5–8.5, and is seen on most vegetated land areas, e.g., mid-high latitudes, which is dominated by reduction in autotrophic respiration. Two-thirds of the change in total respiration comes from the reduction in autotrophic respiration. Terrestrial ecosystem carbon flux is dominated by respiration at night and for deciduous ecosystems, in leafless periods (Valentini et al., 2000). Vegetation dynamics could alter the contribution of the autotrophic respiration to the total respiration (Mukhortova et al., 2021). Increases in C_4 cropland area fraction under SSP5–3.4 appear in the eastern United States, South-eastern South America, Europe, western Central Asia, East Asia, and South Asia.

Increases in disturbance could significantly alter the total biomass and reduce climate resilience (Forzieri et al., 2022; Overpeck et al., 1990). Relative to SSP5–8.5, land use shows strong cropland expansion mainly at the cost of grazing land area under SSP5–3.4, which leads to change in carbon mass flux into atmosphere and contributes to the disturbance (Figure A.17). Increases in C_4 cropland area fraction under SSP5–3.4 appear in the eastern United States, Southeastern South America, Europe, western Central Asia, East Asia, and South Asia, which is associated with bioenergy crop expansion (Melnikova et al., 2022). Disturbance increases by 0.6 ± 0.1 Pg C yr^{-1} under SSP5–3.4 compared with SSP5–8.5 during DJF. The cropland expansion drives the enhancement of carbon turnover and reduces terrestrial carbon uptake driven by the CO_2 fertilization effect, although carbon gains can come from the bioenergy yield without considering energy consumption and emissions capture.

Five of the eight models used in this study include explicit nitrogen cycle coupling in their carbon cycle. UKESM1–0-LL has a land model that simulate vegetation cover dynamically and competition between their plant functional types. In SSP5–3.4 simulations, bioenergy crops were not treated as energy crops definitely but a generic crop vegetation type with high photosynthesis rate grass (Melnikova et al., 2022). Current models include potential scenarios for land use changes (Lawrence et al., 2016), however, land management still lacks a parameterization scheme in the models (Deryng et al., 2016). The carbon cycle exhibits path dependence under aggressive carbon emissions reduction and high levels of overshoot should be used with caution for limiting the environment change (Tokarska et al., 2019), e.g., permafrost thawing, glaciers melting and sea level rise.

Decrease in the terrestrial carbon uptake is caused by a stronger decrease in the photosynthetic carbon absorption than the decrease in the ecosystem respiration, and enhanced disturbance due to biofuel crops expansion under aggressive carbon emissions reduction in the SSP5–3.4 overshoot scenario. The decrease in terrestrial carbon uptake implies that a larger amount of CO_2 would need to be removed to compensate for the part of emissions caused by reduced terrestrial ecosystem absorption under the carbon emissions reduction pathway. This study of seasonal and regional of changes in terrestrial carbon uptake under aggressive carbon emission reduction in an overshoot scenario could provide insights for designing more effective policies for climate change. Future studies should explore the trade-offs between the carbon sinks from the bioenergy yield and carbon releases from land use change disturbance. Natural climate solutions adopting landscape-scale

planning is promising for avoiding greenhouse gas emissions across forests, wetlands, grasslands, and agricultural lands, and enhancing ecological resilience under aggressive carbon emission reduction.

CRediT authorship contribution statement

Wei Cheng: Conceptualization, Formal analysis, Writing – original draft. **Lei Huang:** Data curation, Writing – review & editing, Validation. **Zhu Liu:** Validation, Writing – review & editing. **Jinwei Dong:** Writing – review & editing, Validation. **John C. Moore:** Writing – review & editing, Investigation. **Douglas G. MacMartin:** Writing – review & editing, Investigation. **Xiangzheng Deng:** Conceptualization, Writing – review & editing, Investigation.

Declaration of Competing Interest

The authors declare that they have no known competing financial interests or personal relationships that could have appeared to influence the work reported in this paper.

Data availability

Data from the simulations used in this work can be accessed by https://esgf-node.llnl.gov/search/cmip6/

Acknowledgements

This research is funded by the National Natural Science Foundation of China (Grant No. 72221002). Data analysis and technical validation were supported in part by the Strategic Priority Research Program of Chinese Academy of Sciences (Grant No. XDA23070400) and the National Program on Key Research Projects (Grant No. 2016YFA0602500, 2017YFA0603703).

Supplementary materials

Supplementary material associated with this article can be found, in the online version, at doi:10.1016/j.resconrec.2023.106997.

References

Amiro, B.D., Barr, A.G., Barr, J.G., Black, T.A., Bracho, R., Brown, M., Chen, J., Clark, K. L., Davis, K.J., Desai, A.R., Dore, S., Engel, V., Fuentes, J.D., Goldstein, A.H., Goulden, M.L., Kolb, T.E., Lavigne, M.B., Law, B.E., Margolis, H.A., Martin, T., McCaughey, J.H., Misson, L., Montes-Helu, M., Noormets, A., Randerson, J.T., Starr, G., Xiao, J., 2010. Ecosystem carbon dioxide fluxes after disturbance in forests of North America. J. Geophys. Res.-Biogeosci. 115, G00K02 https://doi.org/10.1029/2010JG001390.

Arora, V.K., Katavouta, A., Williams, R.G., Jones, C.D., Brovkin, V., Friedlingstein, P., Schwinger, J., Bopp, L., Boucher, O., Cadule, P., Chamberlain, M.A., Christian, J.R., Delire, C., Fisher, R.A., Hajima, T., Ilyina, T., Joetzjer, E., Kawamiya, M., Koven, C. D., Krasting, J.P., Law, R.M., Lawrence, D.M., Lenton, A., Lindsay, K., Pongratz, J., Raddatz, T., Séférian, R., Tachiiri, K., Tjiputra, J.F., Wiltshire, A., Wu, T., Ziehn, T., 2020. Carbon–concentration and carbon–climate feedbacks in CMIP6 models and their comparison to CMIP5 models. Biogeosciences 17, 4173–4222. https://doi.org/10.5194/bg-17-4173-2020.

Bony, S., Bellon, G., Klocke, D., Sherwood, S., Fermepin, S., Denvil, S., 2013. Robust direct effect of carbon dioxide on tropical circulation and regional precipitation. Nat. Geosci. 6, 447–451. https://doi.org/10.1038/ngeo1799.

Cao, L., Caldeira, K., 2010. Atmospheric carbon dioxide removal: long-term consequences and commitment. Environ. Res. Lett. 5, 024011 https://doi.org/10.1088/1748-9326/5/2/024011.

Carey, J.C., Tang, J., Templer, P.H., Kroeger, K.D., Crowther, T.W., Burton, A.J., Dukes, J.S., Emmett, B., Frey, S.D., Heskel, M.A., Jiang, L., Machmuller, M.B., Mohan, J., Panetta, A.M., Reich, P.B., Reinsch, S., Wang, X., Allison, S.D., Bamminger, C., Bridgham, S., Collins, S.L., de Dato, G., Eddy, W.C., Enquist, B.J., Estiarte, M., Harte, J., Henderson, A., Johnson, B.R., Larsen, K.S., Luo, Y., Marhan, S., Melillo, J.M., Peñuelas, J., Pfeifer-Meister, L., Poll, C., Rastetter, E., Reinmann, A.B., Reynolds, L.L., Schmidt, I.K., Shaver, G.R., Strong, A.L., Suseela, V., Tietema, A., 2016. Temperature response of soil respiration largely unaltered with experimental warming. Proc. Natl. Acad. Sci. U. S. A. 113, 13797–13802. https://doi.org/10.1073/pnas.1605365113.

Chen, C., Riley, W.J., Prentice, I.C., Keenan, T.F., 2022. CO_2 fertilization of terrestrial photosynthesis inferred from site to global scales. Proc. Natl. Acad. Sci. U. S. A. 119, https://doi.org/10.1073/pnas.2115627119 e2115627119.

Cheng, W., MacMartin, D.G., Kravitz, B., Visioni, D., Bednarz, E.M., Xu, Y., Luo, Y., Huang, L., Hu, Y., Staten, P.W., Hitchcock, P., Moore, J.C., Guo, A., Deng, X., 2022a. Changes in Hadley circulation and intertropical convergence zone under strategic stratospheric aerosol geoengineering. npj. Clim. Atmos. Sci. 5, 32. https://doi.org/10.1038/s41612-022-00254-6.

Cheng, W., Duan, X., Moore, J.C., Deng, X., Luo, Y., Huang, L., Wang, Y., 2022b. Unevenly distributed CO_2 and its impacts on surface energy balance. Atmos. Res. 274, 106196 https://doi.org/10.1016/j.atmosres.2022.106196.

Ciais, P., Reichstein, M., Viovy, N., Granier, A., Ogée, J., Allard, V., Aubinet, M., Buchmann, N., Bernhofer, C., Carrara, A., Chevallier, F., De Noblet, N., Friend, A.D., Friedlingstein, P., Grünwald, T., Heinesch, B., Keronen, P., Knohl, A., Krinner, G., Loustau, D., Manca, G., Matteucci, G., Miglietta, F., Ourcival, J.M., Papale, D., Pilegaard, K., Rambal, S., Seufert, G., Soussana, J.F., Sanz, M.J., Schulze, E.D., Vesala, T., Valentini, R., 2005. Europe-wide reduction in primary productivity caused by the heat and drought in 2003. Nature 437, 529–533. https://doi.org/10.1038/nature03972.

Clark, W.C., 1982. Carbon Dioxide Review 1982. Oxford University Press, Clarendon, England.

Deryng, D., Elliott, J., Folberth, C., Müller, C., Pugh, T.A.M., Boote, K.J., Conway, D., Ruane, A.C., Gerten, D., Jones, J.W., Khabarov, N., Olin, S., Schaphoff, S., Schmid, E., Yang, H., Rosenzweig, C., 2016. Regional disparities in the beneficial effects of rising CO_2 concentrations on crop water productivity. Nat. Clim. Chang. 6, 786–790. https://doi.org/10.1038/nclimate2995.

Forzieri, G., Dakos, V., McDowell, N.G., Ramdane, A., Cescatti, A., 2022. Emerging signals of declining forest resilience under climate change. Nature 608, 534–539. https://doi.org/10.1038/s41586-022-04959-9.

Forzieri, G., Girardello, M., Ceccherini, G., Spinoni, J., Feyen, L., Hartmann, H., Beck, P. S.A., Camps-Valls, G., Chirici, G., Mauri, A., Cescatti, A., 2021. Emergent vulnerability to climate-driven disturbances in European forests. Nat. Commun. 12, 1081. https://doi.org/10.1038/s41467-021-21399-7.

Fuss, S., Canadell, J.G., Peters, G.P., Tavoni, M., Andrew, R.M., Ciais, P., Jackson, R.B., Jones, C.D., Kraxner, F., Nakicenovic, N., Le Quéré, C., Raupach, M.R., Sharifi, A., Smith, P., Yamagata, Y., 2014. Betting on negative emissions. Nat. Clim. Chang. 4, 850–853. https://doi.org/10.1038/nclimate2392.

Gentine, P., Green, J.K., Guerin, M., Humphrey, V., Seneviratne, S.I., Zhang, Y., Zhou, S., 2019. Coupling between the terrestrial carbon and water cycles-a review. Environ. Res. Lett. 14, 083003 https://doi.org/10.1088/1748-9326/ab22d6.

Giardina, C.P., Litton, C.M., Crow, S.E., Asner, G.P., 2014. Warming-related increases in soil CO_2 efflux are explained by increased below-ground carbon flux. Nat. Clim. Chang. 4, 822–827. https://doi.org/10.1038/nclimate2322.

Green, J.K., Seneviratne, S.I., Berg, A.M., Findell, K.L., Hagemann, S., Lawrence, D.M., Gentine, P., 2019. Large influence of soil moisture on long-term terrestrial carbon uptake. Nature 565, 476–479. https://doi.org/10.1038/s41586-018-0848-x.

Hawkes, C.V., Waring, B.G., Rocca, J.D., Kivlin, S.N., 2017. Historical climate controls soil respiration responses to current soil moisture. Proc. Natl. Acad. Sci. U. S. A. 114, 6322–6327. https://doi.org/10.1073/pnas.1620811114.

Hu, Z., Piao, S., Knapp, A.K., Wang, X., Peng, S., Yuan, W., Running, S., Mao, J., Shi, X., Ciais, P., Huntzinger, D.N., Yang, J., Yu, G., 2022. Decoupling of greenness and gross primary productivity as aridity decreases. Remote Sens. Environ. 279, 113120 https://doi.org/10.1016/j.rse.2022.113120.

Hurtt, G.C., Chini, L., Sahajpal, R., Frolking, S., Bodirsky, B.L., Calvin, K., Doelman, J.C., Fisk, J., Fujimori, S., Goldewijk, K.K., Hasegawa, T., Havlik, P., Heinimann, A., Humpenöder, F., Jungclaus, J., Kaplan, J., Kennedy, J., Kristzin, T., Lawrence, D., Lawrence, P., Ma, L., Mertz, O., Pongratz, J., Popp, A., Poulter, B., Riahi, K., Shevliakova, E., Stehfest, E., Thornton, P., Tubiello, F.N., van Vuuren, D.P., Zhang, X., 2020. Harmonization of global land-use change and management for the period 850–2100 (LUH2) for CMIP6. Geosci. Model Dev. 13, 5425–5464. https://doi.org/10.5194/gmd-13-5425-2022.

IPCC, 2021. Climate Change 2021: The Physical Science Basis. Contribution of Working Group I to the Sixth Assessment Report of the Intergovernmental Panel on Climate Change. Cambridge University Press, Cambridge, United Kingdom and New York, NY, USA.

Iturbide, M., Gutiérrez, J.M., Alves, L.M., Bedia, J., Cerezo-Mota, R., Cimadevilla, E., Cofiño, A.S., Di Luca, A., Faria, S.H., Gorodetskaya, I.V., Hauser, M., Herrera, S., Hennessy, K., Hewitt, H.T., Jones, R.G., Krakovska, S., Manzanas, R., Martínez-Castro, D., Narisma, G.T., Nurhati, I.S., Pinto, I., Seneviratne, S.I., van den Hurk, B., Vera, C.S., 2020. An update of IPCC climate reference regions for subcontinental analysis of climate model data: definition and aggregated datasets. Earth Syst. Sci. Data 12, 2959–2970. https://doi.org/10.5194/essd-12-2959-2020.

Jones, C.D., Ciais, P., Davis, S.J., Friedlingstein, P., Gasser, T., Peters, G.P., Rogelj, J., Vuuren, D.P.van, Canadell, J.G., Cowie, A., Jackson, R.B., Jonas, M., Kriegler, E., Littleton, E., Lowe, J.A., Milne, J., Shrestha, G., Smith, P., Torvanger, A., Wiltshire, A., 2016. Simulating the earth system response to negative emissions. Environ. Res. Lett. 11, 095012 https://doi.org/10.1088/1748-9326/11/9/095012.

Jones, C.D., Friedlingstein, P., 2020. Quantifying process-level uncertainty contributions to TCRE and carbon budgets for meeting Paris Agreement climate targets. Environ. Res. Lett. 15, 074019 https://doi.org/10.1088/1748-9326/ab858a.

Jung, M., Reichstein, M., Margolis, H.A., Cescatti, A., Richardson, A.D., Arain, M.A., Arneth, A., Bernhofer, C., Bonal, D., Chen, J., Gianelle, D., Gobron, N., Kiely, G., Kutsch, W., Lasslop, G., Law, B.E., Lindroth, A., Merbold, L., Montagnani, L., Moors, E.J., Papale, D., Sottocornola, M., Vaccari, F., Williams, C., 2011. Global patterns of land-atmosphere fluxes of carbon dioxide, latent heat, and sensible heat

derived from eddy covariance, satellite, and meteorological observations. J. Geophys. Res.-Biogeosci. 116, G00J07 https://doi.org/10.1029/2010JG001566.
Keller, D.P., Lenton, A., Scott, V., Vaughan, N.E., Bauer, N., Ji, D., Jones, C.D., Kravitz, B., Muri, H., Zickfeld, K., 2018. The carbon dioxide removal model intercomparison project (CDRMIP): rationale and experimental protocol for CMIP6. Geosci. Model Dev. 11, 1133–1160. https://doi.org/10.5194/gmd-11-1133-2018.
Konapala, G., Mishra, A.K., Wada, Y., Mann, M.E., 2020. Climate change will affect global water availability through compounding changes in seasonal precipitation and evaporation. Nat. Commun. 11, 3044. https://doi.org/10.1038/s41467-020-16757-w.
Koven, C.D., Arora, V.K., Cadule, P., Fisher, R.A., Jones, C.D., Lawrence, D.M., Lewis, J., Lindsay, K., Mathesius, S., Meinshausen, M., Mills, M., Nicholls, Z., Sanderson, B.M., Séférian, R., Swart, N.C., Wieder, W.R., Zickfeld, K., 2022. Multi-century dynamics of the climate and carbon cycle under both high and net negative emissions scenarios. Earth Syst. Dynam. 13, 885–909. https://doi.org/10.5194/esd-13-885-2022.
Kriegler, E., Bauer, N., Popp, A., Humpenöder, F., Leimbach, M., Strefler, J., Baumstark, L., Bodirsky, B.L., Hilaire, J., Klein, D., Mouratiadou, I., Weindl, I., Bertram, C., Dietrich, J.-P., Luderer, G., Pehl, M., Pietzcker, R., Piontek, F., Lotze-Campen, H., Biewald, A., Bonsch, M., Giannousakis, A., Kreidenweis, U., Müller, C., Rolinski, S., Schultes, A., Schwanitz, J., Stevanovic, M., Calvin, K., Emmerling, J., Fujimori, S., Edenhofer, O., 2017. Fossil-fueled development (SSP5): an energy and resource intensive scenario for the 21st century. Glob. Environ. Change 42, 297–315. https://doi.org/10.1016/j.gloenvcha.2016.05.015.
Lawrence, D.M., Hurtt, G.C., Arneth, A., Brovkin, V., Calvin, K.V., Jones, A.D., Jones, C. D., Lawrence, P.J., Noblet-Ducoudré, N.de, Pongratz, J., Seneviratne, S.I., Shevliakova, E., 2016. The land use model intercomparison project (LUMIP) contribution to CMIP6: rationale and experimental design. Geosci. Model Dev. 9, 2973–2998. https://doi.org/10.5194/gmd-9-2973-2016.
Lei, J., Guo, X., Zeng, Y., Zhou, J., Gao, Q., Yang, Y., 2021. Temporal changes in global soil respiration since 1987. Nat. Commun. 12, 403. https://doi.org/10.1038/s41467-020-20616-z.
Li, D., Zhou, X., Wu, L., Zhou, J., Luo, Y., 2013. Contrasting responses of heterotrophic and autotrophic respiration to experimental warming in a winter annual-dominated prairie. Glob. Change Biol. 19, 3553–3564. https://doi.org/10.1111/gcb.12273.
Melnikova, I., Boucher, O., Cadule, P., Ciais, P., Gasser, T., Quilcaille, Y., Shiogama, H., Tachiiri, K., Yokohata, T., Tanaka, K., 2021. Carbon cycle response to temperature overshoot beyond 2 °C: an analysis of CMIP6 models. Earth Future 9,. https://doi.org/10.1029/2020EF001967 e2020EF001967.
Melnikova, I., Boucher, O., Cadule, P., Tanaka, K., Gasser, T., Hajima, T., Quilcaille, Y., Shiogama, H., Séférian, R., Tachiiri, K., Vuichard, N., Yokohata, T., Ciais, P., 2022. Impact of bioenergy crop expansion on climate-carbon cycle feedbacks in overshoot scenarios. Earth Syst. Dynam. 13, 779–794. https://doi.org/10.5194/esd-13-779-2022.
Minx, J.C., Lamb, W.F., Callaghan, M.W., Fuss, S., Hilaire, J., Creutzig, F., Amann, T., Beringer, T., Garcia, W.de O., Hartmann, J., Khanna, T., Lenzi, D., Luderer, G., Nemet, G.F., Rogelj, J., Smith, P., Vicente, J.L.V., Wilcox, J., Dominguez, M.del M.Z., 2018. Negative emissions—Part 1: research landscape and synthesis. Environ. Res. Lett. 13, 063001 https://doi.org/10.1088/1748-9326/aabf9b.
Mukhortova, L., Schepaschenko, D., Moltchanova, E., Shvidenko, A., Khabarov, N., See, L., 2021. Respiration of Russian soils: climatic drivers and response to climate change. Sci. Total Environ. 785, 147314 https://doi.org/10.1016/j.scitotenv.2021.147314.
O'Neill, B.C., Tebaldi, C., Vuuren, D.P.van, Eyring, V., Friedlingstein, P., Hurtt, G., Knutti, R., Kriegler, E., Lamarque, J.-F., Lowe, J., Meehl, G.A., Moss, R., Riahi, K., Sanderson, B.M., 2016. The scenario model intercomparison project (ScenarioMIP) for CMIP6. Geosci. Model Dev. 9, 3461–3482. https://doi.org/10.5194/gmd-9-3461-2016.
Overpeck, J.T., Rind, D., Goldberg, R., 1990. Climate-induced changes in forest disturbance and vegetation. Nature 343, 51–53. https://doi.org/10.1038/343051a0.
Pithan, F., Mauritsen, T., 2014. Arctic amplification dominated by temperature feedbacks in contemporary climate models. Nat. Geosci. 7, 181–184. https://doi.org/10.1038/ngeo2071.
Riahi, K., van Vuuren, D.P., Kriegler, E., Edmonds, J., O'Neill, B.C., Fujimori, S., Bauer, N., Calvin, K., Dellink, R., Fricko, O., Lutz, W., Popp, A., Cuaresma, J.C., Kc, S., Leimbach, M., Jiang, L., Kram, T., Rao, S., Emmerling, J., Ebi, K., Hasegawa, T., Havlik, P., Humpenöder, F., Da Silva, L.A., Smith, S., Stehfest, E., Bosetti, V., Eom, J., Gernaat, D., Masui, T., Rogelj, J., Strefler, J., Drouet, L., Krey, V., Luderer, G., Harmsen, M., Takahashi, K., Baumstark, L., Doelman, J.C., Kainuma, M., Klimont, Z., Marangoni, G., Lotze-Campen, H., Obersteiner, M., Tabeau, A., Tavoni, M., 2017. The shared socioeconomic pathways and their energy, land use, and greenhouse gas emissions implications: an overview. Glob. Environ. Change 42, 153–168. https://doi.org/10.1016/j.gloenvcha.2016.05.009.
Rogelj, J., Popp, A., Calvin, K.V., Luderer, G., Emmerling, J., Gernaat, D., Fujimori, S., Strefler, J., Hasegawa, T., Marangoni, G., Krey, V., Kriegler, E., Riahi, K., van Vuuren, D.P., Doelman, J., Drouet, L., Edmonds, J., Fricko, O., Harmsen, M., Havlík, P., Humpenöder, F., Stehfest, E., Tavoni, M., 2018. Scenarios towards limiting global mean temperature increase below 1.5°C. Nat. Clim. Chang. 8, 325–332. https://doi.org/10.1038/s41558-018-0091-3.
Seibold, S., Rammer, W., Hothorn, T., Seidl, R., Ulyshen, M.D., Lorz, J., Cadotte, M.W., Lindenmayer, D.B., Adhikari, Y.P., Aragón, R., Bae, S., Baldrian, P., Barimani Varandi, H., Barlow, J., Bässler, C., Beauchêne, J., Berenguer, E., Bergamin, R.S., Birkemoe, T., Boros, G., Brandl, R., Brustel, H., Burton, P.J., Cakpo-Tossou, Y.T., Castro, J., Cateau, E., Cobb, T.P., Farwig, N., Fernández, R.D., Firn, J., Gan, K.S., González, G., Gossner, M.M., Habel, J.C., Hébert, C., Heibl, C., Heikkala, O., Hemp, A., Hemp, C., Hjältén, J., Hotes, S., Kouki, J., Lachat, T., Liu, J., Liu, Y., Luo, Y.-H., Macandog, D.M., Martina, P.E., Mukul, S.A., Nachin, B., Nisbet, K., O'Halloran, J., Oxbrough, A., Pandey, J.N., Pavlíček, T., Pawson, S.M., Rakotondranary, J.S., Ramanamanjato, J.-B., Rossi, L., Schmidl, J., Schulze, M., Seaton, S., Stone, M.J., Stork, N.E., Suran, B., Sverdrup-Thygeson, A., Thorn, S., Thyagarajan, G., Wardlaw, T.J., Weisser, W.W., Yoon, S., Zhang, N., Müller, J., 2021. The contribution of insects to global forest deadwood decomposition. Nature 597, 77–81. https://doi.org/10.1038/s41586-021-03740-8.
Seidl, R., Thom, D., Kautz, M., Martin-Benito, D., Peltoniemi, M., Vacchiano, G., Wild, J., Ascoli, D., Petr, M., Honkaniemi, J., Lexer, M.J., Trotsiuk, V., Mairota, P., Svoboda, M., Fabrika, M., Nagel, T.A., Reyer, C.P.O., 2017. Forest disturbances under climate change. Nat. Clim. Chang. 7, 395–402. https://doi.org/10.1038/nclimate3303.
Sellar, A.A., Jones, C.G., Mulcahy, J.P., Tang, Y., Yool, A., Wiltshire, A., O'Connor, F.M., Stringer, M., Hill, R., Palmieri, J., Woodward, S., Mora, L.de, Kuhlbrodt, T., Rumbold, S.T., Kelley, D.I., Ellis, R., Johnson, C.E., Walton, J., Abraham, N.L., Andrews, M.B., Andrews, T., Archibald, A.T., Berthou, S., Burke, E., Blockley, E., Carslaw, K., Dalvi, M., Edwards, J., Folberth, G.A., Gedney, N., Griffiths, P.T., Harper, A.B., Hendry, M.A., Hewitt, A.J., Johnson, B., Jones, A., Jones, C.D., Keeble, J., Liddicoat, S., Morgenstern, O., Parker, R.J., Predoi, V., Robertson, E., Siahaan, A., Smith, R.S., Swaminathan, R., Woodhouse, M.T., Zeng, G., Zerroukat, M., 2019. UKESM1: description and evaluation of the U.K. earth system model. J. Adv. Model. Earth Syst. 11, 4513–4558. https://doi.org/10.1029/2019MS001739.
Senf, C., Buras, A., Zang, C.S., Rammig, A., Seidl, R., 2020. Excess forest mortality is consistently linked to drought across Europe. Nat. Commun. 11, 6200. https://doi.org/10.1038/s41467-020-19924-1.
Shi, B., Fu, X., Smith, M.D., Chen, A., Knapp, A.K., Wang, C., Xu, W., Zhang, R., Gao, W., Sun, W., 2022. Autotrophic respiration is more sensitive to nitrogen addition and grazing than heterotrophic respiration in a meadow steppe. Catena 213, 106207. https://doi.org/10.1016/j.catena.2022.106207.
Stocker, B.D., Zscheischler, J., Keenan, T.F., Prentice, I.C., Peñuelas, J., Seneviratne, S.I., 2018. Quantifying soil moisture impacts on light use efficiency across biomes. New Phytol. 218, 1430–1449. https://doi.org/10.1111/nph.15123.
Tokarska, K.B., Zickfeld, K., Rogelj, J., 2019. Path independence of carbon budgets when meeting a stringent global mean temperature target after an overshoot. Earth Future 7, 1283–1295. https://doi.org/10.1029/2019EF001312.
Valentini, R., Matteucci, G., Dolman, A.J., Schulze, E.-D., Rebmann, C., Moors, E.J., Granier, A., Gross, P., Jensen, N.O., Pilegaard, K., Lindroth, A., Grelle, A., Bernhofer, C., Grünwald, T., Aubinet, M., Ceulemans, R., Kowalski, A.S., Vesala, T., Rannik, Ü., Berbigier, P., Loustau, D., Guðmundsson, J., Thorgeirsson, H., Ibrom, A., Morgenstern, K., Clement, R., Moncrieff, J., Montagnani, L., Minerbi, S., Jarvis, P.G., 2000. Respiration as the main determinant of carbon balance in European forests. Nature 404, 861–865. https://doi.org/10.1038/35009084.
Wang, K., Bastos, A., Ciais, P., Wang, X., Rödenbeck, C., Gentine, P., Chevallier, F., Humphrey, V.W., Huntingford, C., O'Sullivan, M., Seneviratne, S.I., Sitch, S., Piao, S., 2022. Regional and seasonal partitioning of water and temperature controls on global land carbon uptake variability. Nat. Commun. 13, 3469. https://doi.org/10.1038/s41467-022-31175-w.
Watson, R.T., Noble, I.R., Bolin, B., Ravindranath, N.H., Verardo, D.J., Dokken, D.J., 2000. IPCC Special Report: Land Use, Land-Use Change, and Forestry. Cambridge University Press, Cambridge.
Xia, J., Niu, S., Ciais, P., Janssens, I.A., Chen, J., Ammann, C., Arain, A., Blanken, P.D., Cescatti, A., Bonal, D., Buchmann, N., Curtis, P.S., Chen, S., Dong, J., Flanagan, L.B., Frankenberg, C., Georgiadis, T., Gough, C.M., Hui, D., Kiely, G., Li, J., Lund, M., Magliulo, V., Marcolla, B., Merbold, L., Montagnani, L., Moors, E.J., Olesen, J.E., Piao, S., Raschi, A., Roupsard, O., Suyker, A.E., Urbaniak, M., Vaccari, F.P., Varlagin, A., Vesala, T., Wilkinson, M., Weng, E., Wohlfahrt, G., Yan, L., Luo, Y., 2015. Joint control of terrestrial gross primary productivity by plant phenology and physiology. Proc. Natl. Acad. Sci. U. S. A. 112, 2788–2793. https://doi.org/10.1073/pnas.1413090112.
Zhang, W., Yu, G., Chen, Z., Zhu, X., Han, L., Liu, Z., Lin, Y., Han, S., Sha, L., Wang, H., Wang, Y., Yan, J., Zhang, Y., Gharun, M., 2022. Photosynthetic capacity dominates the interannual variation of annual gross primary productivity in the Northern Hemisphere. Sci. Total Environ. 157856 https://doi.org/10.1016/j.scitotenv.2022.157856.
O'Hara, F.N., 1990. Glossary: carbon dioxide and climate (No. cdiac:CDIAC-039). Environmental system science data infrastructure for a virtual ecosystem (ESS-DIVE) (United States). https://doi.org/10.15485/1463805.